J. Plasma Physics (2002), *vol.* 67, *part* 4, *pp.* 277–299. © 2002 Cambridge University Press
DOI: 10.1017/S0022377802001654 Printed in the United Kingdom

The structure of the double layer behind the Moon

N. BORISOV* and U. MALL

Max-Planck-Institut für Aeronomie, D-37191 Katlenburg-Lindau, Germany

(Received 19 February 2002)

Abstract. The distribution of plasma and electric fields close to the far side of the Moon are discussed. The existence of a strong double layer behind the Moon is predicted and its parameters are investigated. Electric currents associated with this double layer and finite conductivity inside the Moon are estimated. The fluxes of suprathermal electrons behind the Moon in different energy ranges are calculated and compared with the experimental data. It is shown that the theoretical results are in qualitative agreement with the data obtained by Lunar Prospector and the Apollo 15 subsatellite.

1. Introduction

A large body moving in a plasma acquires an electric potential on its surface in order to prevent strong electric charging. This charging has its origin in the different thermal velocities of electrons and ions. This results in the formation of a region of non-neutral plasma consisting of two adjacent space-charge layers, one positively and one negatively charged. Such a structure is generally called a double layer. Inside this layer, quasineutrality is violated. Typically, the transverse scale for double layers is of the order of a few Debye radii.

Many years ago, the existence of a double layer around a large conducting body (a satellite) moving in the ionosphere was discussed theoretically by Al'pert et al. (1965). The potential difference in the double layer depends on many factors (e.g. the thermal speeds of particles, the speed of the body, the interaction of particles with the surface and the electric conductivity of the body). It was shown that in front of the body, the double layer is thin, while behind the body, where the concentration of the charged particles is very small, the transverse dimension of this layer is comparable to the dimension of the body.

It is clear that double layers should also exist around large non-magnetized cosmic bodies, such as the Moon and asteroids, due to the interaction with the solar wind plasma. The most important difference between the two above-mentioned cases lies in the distribution functions of the charged particles of the medium in which the bodies are moving. In the case of the Earth's ionosphere, the distributions of electrons and ions can, under quiet conditions, be described by Maxwellians due to rather frequent collisions, while the distributions of electrons and ions in the

*Permanent address: Institute of Terrestrial Magnetism, Ionosphere and Radio Waves Propagation (IZMIRAN), 142190 Troitsk, Moscow Region, Russia.

https://doi.org/10.1017/S0022377802001654 Published online by Cambridge University Press

solar wind plasma usually show non-Maxwellian tails (see e.g. Anderson et al. 1972; Pilipp et al. 1987; Astudillo et al. 1996; Gloecker et al. 1992).

In the past, work centered on the double layer of the sunlit hemisphere of the Moon: the so-called lunar photoelectron layer (PEL). In this case, photoelectrons are emitted from the lunar surface due to solar ultraviolet photons. Given the fact that the photoemission rate is much greater than the rate of electron accretion from the solar wind, the surface becomes positively charged, thus pulling back most emitted photoelectrons. Since the average photoelectrons do not have the energy to rise against electrostatic forces, an electron layer, the PEL, forms just above the lunar surface. Indeed, the positive potential of the Moon's surface on its sunlit side was measured many years ago by Freeman et al. (1973) and was found to be rather weak (several volts).

While the structure of the double layer at the sunlit side of the Moon was widely discussed in several papers (see e.g. Goldstein 1974; Grobman and Blank 1969), there were no measurements of the electric field distribution on the far side of the Moon nor was the existence and the structure of the double layer behind the Moon discussed in any form. Only recently have measurements made by the Wind spacecraft in the lunar wake at a distance of about seven lunar radii led Ogilvie et al. (1996) to assume the existence of a rather large negative potential in the center of the wake (~ 400 V). One may suspect that closer to the Moon, this electric potential should increase significantly.

The aim of the present paper is to focus on the double layer behind the Moon, which has not been previously discussed in the literature. In addition, we will discuss its formation and structure under stationary conditions. The paper is organized as follows. First, basic equations are derived. The distribution of the electric potential at the far side of the Moon is analyzed in Sec. 3. In Sec. 4, the structure of the double layer behind the Moon is investigated. The behavior of electron fluxes for different energy ranges behind the Moon is discussed in Sec. 5. In Sec. 6, we consider the distribution of the electric fields for arbitrary direction of the magnetic field. The results are then summarized in Sec. 7.

2. Basic equations

Our aim is to investigate the electric field distribution close to the far side of the Moon in its simplest form. For this purpose, we use a two-dimensional model. Imagine a disk inserted in the flow of the solar wind (see Fig. 1). Let the x axis be directed along the solar wind speed $\mathbf{u}_{sw}$. First, we suppose that the magnetic field of the solar wind is orthogonal to the flow velocity $\mathbf{u}_{sw}$ and coincides with the z axis. The axis orthogonal to the disk plain is the y axis. It is convenient to introduce a cylindrical system of coordinates with the radius r and the angle θ measured from the x axis. At the Moon's surface, $r = r_m$. Our two-dimensional model is valid if the deviation of particle trajectories from the disk is small enough. The corresponding condition is given below. In our model, we restrict ourselves to the investigation of the electric potential behind the Moon, where the flux of photoelectrons is absent. In addition, we assume that all charged particles that collide with the lunar surface are absorbed. It is obvious that if all incident particles had the same velocity $\mathbf{u}_{sw}$ then a region of rarefaction would appear behind the Moon. A filling of this particle depleted region can occur only when particles have a velocity component v_z in a direction perpendicular to the incoming bulk velocity $\mathbf{u}_{sw}$. From a geometrical

https://doi.org/10.1017/S0022377802001654 Published online by Cambridge University Press

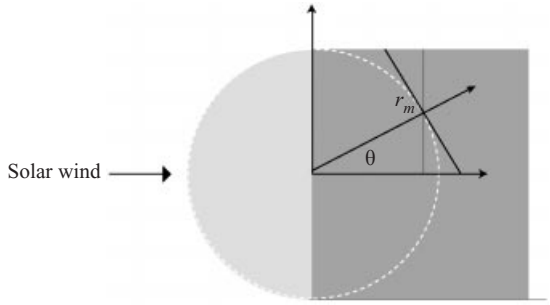


Figure 1. Schematic of the geometry used in the model.

argument (see Fig. 1), one easily finds that in order to collide with the surface on the far side of the Moon, the velocity component $|v_z|$ of a neutral particle must fulfill the inequality

$$|v_z| > (u_{sw} + v_x)\cot|\theta|, \tag{1}$$

where $|\theta| < \pi/2$ (since we only discuss the distribution of the electric potential on the far side of the Moon). This means that the smaller the angle θ becomes, the higher the speed of a particle $|v_z|$ must be to reach the corresponding surface point. Put simply: only fast particles can reach the surface of the Moon on its dark side. In other words, the electron and ion fluxes hitting the Moon on its far side ($|\theta| < \pi/2$) are strongly determined by the form of its distribution functions in the solar wind. Since the conductivity of the Moon near its surface is low (Dyal et al. 1974) and the thermal speeds of electrons (v_{Te}) and ions (v_{Ti}) in the solar wind are so different ($v_{Ti} \ll u_{sw} \ll v_{Te}$), an electric potential builds up on the far side of the Moon. This then explains why the existence of non-Maxwellian tails in the distribution functions can significantly alter the electric potential behind the Moon. Since the undisturbed flux of electrons along the magnetic field line is much larger than the ion flux, the potential on the dark side of the Moon should be negative.

Distribution functions of protons and electrons in the solar wind are rather variable. Normally, they consist of a Maxwellian core and a non-Maxwellian halo. Different approximations have been used to describe the high-energy tails. From electron flux measurements taken by the Apollo 15 subsatellite behind the Moon, we know that high-energy tails can be approximated by power laws (Anderson et al. 1972). The same type of distribution is often used to characterize fast protons in the solar wind (Gloecker et al. 1992). With the aim of simplifying our calculations, we choose the following distribution functions in the undisturbed solar wind for electrons (F_e) and for protons (F_i):

$$F_e = \frac{N_0}{(\sqrt{2\pi}v_{Te})^3} e^{-v^2/2v_{Te}^2} + \mu_e \frac{N_0}{(\sqrt{2\pi}v_{eH})^3} \left(\frac{2v_{eH}^2}{v_z^2 + 2v_{eH}^2}\right)^n e^{-v_\perp^2/2v_{eH}^2}, \tag{2}$$

$$F_i = \frac{N_0}{(\sqrt{2\pi}v_{Ti})^3} e^{-v^2/2v_{Ti}^2} + \mu_i \frac{N_0}{(\sqrt{2\pi}v_{iH})^3} \left(\frac{2v_{iH}^2}{v_z^2 + 2v_{iH}^2}\right)^m e^{-v_\perp^2/2v_{iH}^2}. \tag{3}$$

Here N_0 is the concentration of the thermal plasma in the solar wind, $\mu_\alpha N_0$ are the small fractions that correspond to high-energy tails ($\alpha = i, e$), v_{Te} and v_{Ti} are the thermal speeds of electrons and protons, and v_{eH} and v_{iH} are the corresponding characteristic speeds in the halo. The quantities $n \sim m$ describe the power law

https://doi.org/10.1017/S0022377802001654 Published online by Cambridge University Press

spectra along the magnetic field lines (usually $3 \leqslant n, m \leqslant 5$); $v_\perp^2 = v_x^2 + v_y^2$ is the square of the transverse velocity and $v^2 = v_x^2 + v_y^2 + v_z^2$ is the square of the total velocity.

To find the electric potential in the region along the far side of the Moon, we need to solve the Poisson equation. As a second-order partial differential equation, we need to specify two boundary conditions. One boundary condition is determined by the electric potential on the surface of the Moon. The second boundary condition is established at the rear boundary of the layer, where quasineutrality is restored. Now we proceed to find the first boundary condition. For this purpose, we have to calculate electron and proton fluxes directed towards the Moon at its rear side. Since under stationary conditions the conservation of the electric current I is valid at each point on the surface of the Moon, we can write

$$\boldsymbol{\nabla} \cdot \mathbf{I} = 0. \tag{4}$$

From the integration of (4) across the surface of the Moon, it follows that the total current (as a sum of the radial component of the ion current eJ_{ir} and electron current $-eJ_{er}$) outside and inside of the Moon must be equal:

$$-\sigma_m \frac{\partial \phi}{\partial r}\bigg|_{r_m} = e[J_{ir}(\theta, r_m) - J_{er}(\theta, r_m, \phi)]. \tag{5}$$

Here σ_m is the conductivity of the Moon on its surface, $-e$ is the charge of the electron, J_{ir} and J_{er} are the radial fluxes of ions and electrons, and ϕ is the electric potential.

To calculate the radial component of the ion flux J_{ir} and electron flux J_{er} hitting a particle point (described by θ) on the far side of the Moon, the appropriate longitudinal velocity components to reach this point must be known. Because ions and electrons respond differently to the appearance of a large negative electric potential behind the Moon, we have to calculate the ion and electron fluxes separately.

For the calculation of the ion flux, we can directly apply (1), where $\theta > 0$, since we want to discuss the distribution of the electric potential only for positive angles. For negative angles, the result changes symmetrically. Knowing the velocity constraint, we need to find out whether or not ions can be treated as free particles. This is the case if the time to reach the surface point is small compared with the gyration period $\tau \ll 2\pi/\omega_{Hi}$, where ω_{Hi} is the gyrofrequency of protons in the solar wind.

The minimal time interval Δt_i required for protons to reach a point on the surface with coordinates (r_m, θ) from the undisturbed solar wind is a function of their longitudinal velocity. Using (1), we arrive at the following approximate result:

$$\Delta t_i \leqslant \tau(\theta) = \frac{r_m(1 - \sin\theta)}{u_{sw} \cot\theta}. \tag{6}$$

Figure 2 shows $\tau(\theta)$ for a moderate solar wind speed of $u_{sw} = 400\,\mathrm{km\,s^{-1}}$. This time is small compared with the gyration period $\tau \ll 2\pi/\omega_{Hi}$ of protons in the solar wind; hence, the ions can indeed be treated as free (non-gyrating) particles. This is why our two-dimensional model is valid for ions. Such a model is also valid for electrons if their motion with the drift velocity v_d during the period of penetration Δt_e is much smaller than the scale of inhomogeneity (of the order of the Lunar radius r_m): $v_d \Delta t_e \ll r_m$.

Since only very fast ions can reach the far side of the Moon, the influence of the electric potential on the motion of such ions can be neglected. It means that the

https://doi.org/10.1017/S0022377802001654 Published online by Cambridge University Press

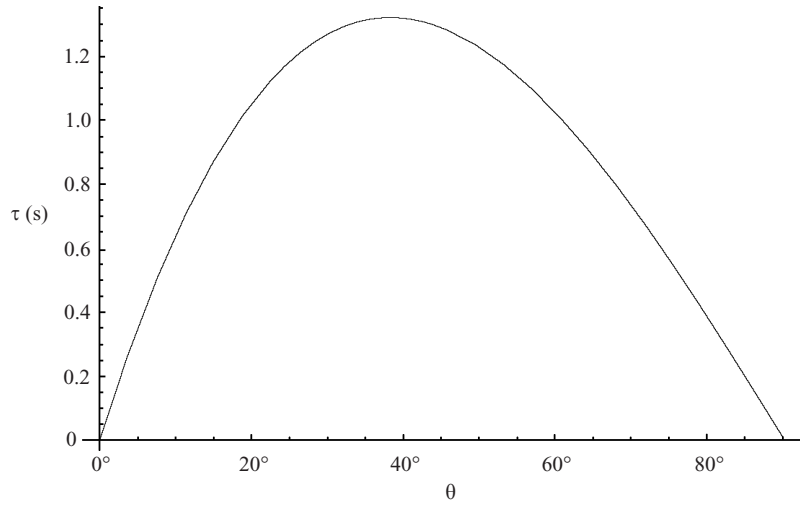


Figure 2. The characteristic time interval (in seconds) required for protons to reach the far side of the Moon with the coordinates (r_m, θ) from the undisturbed solar wind. The solar wind velocity $u_{sw} = 410\,\mathrm{km\,s^{-1}}$.

expression for the radial component of the ion flux J_{ir} is then obtained if we take the velocity component normal to the surface and integrate it with the undisturbed distribution function (2):

$$J_{ir} = \int_{-\infty}^{0} dv_z \int_{-\infty}^{-(v_z \tan\theta + u_{sw})} [v_z \sin\theta + (u_{sw} + v_x)\cos\theta]\, dv_x \int_{-\infty}^{\infty} F_i\, dv_y. \quad (7)$$

The domain of integration in velocity space is determined by (1): $v_z \sin\theta + v_x \cos\theta \leqslant -u_{sw}\cos\theta$, $-\infty \leqslant v_y \leqslant \infty$. After integration with respect to v_x and v_y, we find the flux of ions as a one-dimensional integral:

$$J_{ir}(\theta) = -\frac{N_0}{\sqrt{2}\pi} v_{Ti} \cos\theta \int_0^{\infty} e^{-\zeta_{i,1}^2} [e^{-\chi_{i,1}^2} - \sqrt{\pi}\chi_{i,1}\,\mathrm{Erfc}(\chi_{i,1})]\, d\zeta_{i,1}$$
$$-\mu_i \frac{N_0}{\sqrt{2}\pi} v_{iH} \cos\theta \int_0^{\infty} \frac{1}{(\zeta_{i,2}^2 + 1)^3} [e^{-\chi_{i,2}^2} - \sqrt{\pi}\chi_{i,2}\,\mathrm{Erfc}(\chi_{i,2})]\, d\zeta_{i,2}. \quad (8)$$

Here we have taken

$$m = 3, \qquad \zeta_{i,1} = -\frac{v_z}{\sqrt{2}v_{Ti}}, \qquad \zeta_{i,2} = -\frac{v_z}{\sqrt{2}v_{iH}},$$
$$\chi_{i,1} = U_{i,1} - \zeta_{i,1}\tan\theta, \qquad \chi_{i,2} = U_{i,2} - \zeta_{i,2}\tan\theta,$$

$$U_{i,1} = \frac{u_{sw}}{\sqrt{2}v_{Ti}}, \qquad U_{i,2} = \frac{u_{sw}}{\sqrt{2}v_{iH}};$$

$\mathrm{Erfc}(x) = 1 - \mathrm{Erf}(x)$, where $\mathrm{Erf}(x) = (2/\sqrt{\pi}) \int_0^x e^{-t^2}\, dt$ is the error function. The minus sign in (8) appears because the flux is directed towards the Moon.

Note that large parameters $U_{i,1} \gg 1$ and $U_{i,2} \gg 1$ enter the expression (8). Due

https://doi.org/10.1017/S0022377802001654 Published online by Cambridge University Press

to this, an approximate analytical result for J_{ir} follows from (8):

$$J_{ir}(\theta) \approx -\frac{N_0 v_{Ti}}{\sqrt{2\pi}}[0.5\cos^2\theta\, e^{-U_{i,1}^2\cos^2\theta}\,\mathrm{Erfc}(-U_{i,1}\sin\theta)]$$
$$-\frac{N_0 v_{Ti}}{\sqrt{2\pi}}[\sin\theta\, e^{-U_{i,1}^2/\tan^2\theta} - 1.77U_{i,1}\cos\theta\,\mathrm{Erfc}(U_{i,1}/\tan\theta)]$$
$$-\frac{\mu_i}{\sqrt{2\pi}}N_0 v_{iH}\cos\theta\left[A - 2U_{i,2}\int_{U_{i,2}/\tan\theta}^{\infty}\frac{1}{(\zeta_{i,2}^2+1)^3}\,d\zeta_{i,2}\right], \tag{9}$$

where

$$A = \frac{\tan^5\theta}{(U_{i,2}^2+\tan^2\theta)^3} + 0.5\frac{\tan^5\theta}{(U_{i,2}^2+\tan^2\theta)^2}.$$

In our analysis, we have not calculated the ion flux J_{ir} in a self-consistent way, since only very fast ions can reach the far side of the Moon. As shown below, the electric potential ϕ is not strong enough to significantly influence the motion of such fast ions: $|e\phi| < Mu_{sw}^2\cot^2\theta/2$. Therefore, we neglect perturbations in the motion of ions due to such a potential.

We now turn to the calculation of the electron flux. Under stationary conditions, the total energy of electrons moving in the magnetic field and a potential electric field $\mathbf{E} = -\boldsymbol{\nabla}\phi$ is conserved. As the gyroradius of electrons ρ_{He} is much smaller than the scale of inhomogeneity, the averaged magnetic moment of electrons is an adiabatic invariant. Hence, the longitudinal energy of electrons is conserved:

$$v_z^2 - \frac{2e\phi}{m} = \text{const.} \tag{10}$$

In calculating the flux of electrons, we use the guiding center approximation. The trajectory of an electron near the far side of the Moon in the lowest approximation with respect to the gyroradius is determined by its equation of motion, which can be expressed with the help of (10) in the form

$$\frac{dx}{u_{sw}} = -\frac{dz}{\sqrt{v_{0,e}^2 + 2e\phi/m}}, \tag{11}$$

where $v_{0,e}$ is the initial v_z component of the electron speed in the undisturbed region. We need to find for a given point (z,x) the minimum speed of an electron $v_{z,m}^{(e)}$ that reaches this point and whose trajectory does not intersect the surface of the Moon. Note that the potential ϕ is a function of both coordinates (z,x). This makes the problem rather complicated, because the potential ϕ is not a given function, but needs to be determined.

Therefore, as a first step, we use a simple approximate analytical approach. To find the radial component of the electron flux, we need to know the electron distribution function behind the Moon in the presence of the electric potential ϕ and the limits of integration with respect to the v_z component. The validity of (10) means that in the electron distribution function (2), we only need to substitute

$$v_z^2 \to v_z^2 + \frac{2e\phi}{m}. \tag{12}$$

The lower limit of integration $v_{z,m}^{(e)}$ is an unknown, non-local function of the potential ϕ. Let $\zeta_{e,1}^{(m)}$ and $\zeta_{e,2}^{(m)}$ be two characteristic, dimensionless speeds associated

https://doi.org/10.1017/S0022377802001654 Published online by Cambridge University Press

with this limiting velocity:

$$\zeta_{e,1}^{(m)} = -\frac{v_{z,m}^{(e)}}{\sqrt{2}v_{Te}}, \qquad \zeta_{e,2}^{(m)} = -\frac{v_{z,m}^{(e)}}{\sqrt{2}v_{eH}}.$$

The radial component of the electron flux can be expressed as

$$J_{er} = -\frac{N_0 v_{Te}}{\sqrt{2}\pi} e^{e\phi/T_e} \cos\theta \int_{\zeta_{e,1}^{(m)}}^{\infty} e^{-\zeta_{e,1}^2} [e^{-\chi_{e,1}^2} - \sqrt{\pi}\chi_{e,1} \operatorname{Erfc}(\chi_{e,1})]\, d\zeta_{e,1}$$
$$-\mu_e \frac{N_0}{\sqrt{2}\pi} v_{eH} \cos\theta \int_{\zeta_{e,2}^{(m)}}^{\infty} \frac{1}{(\zeta_{e,2}^2 - e\phi/T_{eH} + 1)^5} [e^{-\chi_{e,2}^2} - \sqrt{\pi}\chi_{e,2} \operatorname{Erfc}(\chi_{e,2})]\, d\zeta_{e,2}. \tag{13}$$

Here

$$\zeta_{e,1} = -\frac{v_z}{\sqrt{2}v_{Te}}, \qquad \zeta_{e,2} = -\frac{v_z}{\sqrt{2}v_{eH}},$$
$$\chi_{e,1} = U_{e,1} - \zeta_{e,1}\tan\theta, \qquad \chi_{e,2} = U_{e,2} - \zeta_{e,2}\tan\theta,$$
$$U_{e,1} = \frac{u_{sw}}{\sqrt{2}v_{Te}}, \qquad U_{e,2} = \frac{u_{sw}}{\sqrt{2}v_{eH}}.$$

Note that, in accordance with the measurements, we have taken $n = 5$ (see Anderson et al. 1972). If we neglect the influence of the potential ϕ on the limiting speeds $\zeta_{e,1}^{(m)}$ and $\zeta_{e,2}^{(m)}$, we find that, according to (12), they are equal to $\zeta_{e,1}^{(m)} = U_{e,1}/\tan\theta$ and $\zeta_{e,2}^{(m)} = U_{e,2}/\tan\theta$. Since the potential ϕ is negative, electrons are losing energy. Hence, in reality, the speeds $\zeta_{e,1}^{(m)}$ and $\zeta_{e,2}^{(m)}$ should be somewhat larger than those mentioned above. The expression (13) can be simplified due to the existence of small parameters $\zeta_{e,1}^{(m)} \ll 1$ and $\zeta_{e,2}^{(m)} \ll 1$. In the case when $\zeta_{e,1}^{(m)} = U_{e,1}/\tan\theta$ and $\zeta_{e,2}^{(m)} = U_{e,2}/\tan\theta$, we arrive at the following result:

$$J_{er} \approx -\frac{N_0 v_{Te}}{\sqrt{2\pi}} e^{-F} [0.5\cos^2\theta\, e^{-U_{e,1}^2\cos^2\theta} \operatorname{Erfc}(U_{e,1}\cos^2\theta/\sin\theta)]$$
$$-\frac{N_0 v_{Te}}{\sqrt{2\pi}} e^{-F} [\sin\theta\, e^{-U_{e,1}^2/\tan^2\theta} - \sqrt{\pi}U_{e,1}\cos\theta \operatorname{Erfc}(U_{e,1}/\tan\theta)]$$
$$-\frac{\mu_e N_0 v_{eH}}{\sqrt{2}\pi} \left\{ \frac{\sqrt{\pi}}{4} \sin\theta \tan^8\theta \left[U_{e,2}^2 + \tan^2\theta \left(1 + F\frac{v_{Te}^2}{v_{eH}^2} \right) \right]^{-4} \right.$$
$$\left. + \cos\theta \tan^9\theta \Phi_e(\phi,\theta) \right\} \tag{14}$$

where

$$\Phi_e = \int_{U_{e,2}}^{\infty} \frac{e^{-z^2}\, dz}{(z^2 + (1 + Fv_{Te}^2/v_{eH}^2)\tan^2\theta)^5}, \qquad F = -\frac{e\phi}{T_e}.$$

3. Electric potential along the surface of the far side of the Moon

3.1. Zero conductivity

Having found the analytical expressions for the electron and proton fluxes, we can distinguish two cases. In the case where the surface of the Moon is considered an

https://doi.org/10.1017/S0022377802001654 Published online by Cambridge University Press

insulator, the flux of ions (8) has to equal the flux of electrons (13) everywhere along the surface of the Moon with $r = r_m$ at its far side:

$$J_{ir}(\theta, r_m) = J_{er}(\theta, r_m, \phi). \tag{15}$$

The absolute value of the potential is determined by (15). An approximate analytical formula for the non-dimensional potential $F = -e\phi/T_e$ is obtained by equating the fluxes of suprathermal protons and electrons:

$$F(\theta) \approx 0.9 U_{i,2} \frac{v_{eH}^2}{v_{Te}^2} \left(\frac{v_{eH}}{v_{iH}} \right)^{1/4} \cot\theta. \tag{16}$$

One sees that as θ tends towards zero, the potential increases as $\sim \cot\theta$.

In the case where the real conductivity of the Moon near its surface is small but finite (Dyal et al. 1974), a small lunar conductivity influences the distribution of the electric potential, since the electron and ion fluxes at the dark side of the Moon are rather low and, at the same time, the electric potential is quite high. In general, the conductivity σ_m is a function of the coordinates. It is believed that the conductivity σ_m increases rapidly towards the center of the Moon. Models containing several layers with different conductivities were discussed by Dyal et al. (1974), Kuckes (1971) and Sonett and Mihalov (1972). Still, there is a rather large uncertainty in the predictions of different authors (Lin et al. 1998). According to Dyal et al. (1974) and Lin et al. (1998), the conductivity grows rapidly inside the Moon from $\sigma_m(r_m) \approx 10^{-10}$–$10^{-9}\,\mathrm{S\,m^{-1}}$ to the order of $10^{-4}\,\mathrm{S\,m^{-1}}$ at a depth of approximately 200 km. In addition, we use a simple model, assuming that the conductivity σ_m grows exponentially in the lunar crust with $r_1 \leqslant r \leqslant r_m$ and becomes infinite for smaller distances from the center with $r < r_1$. Equations (5), (8) and (13) allow us to investigate the distribution of the electric potential on the far side of the Moon for different values of the main parameters $\sigma_m(r_m)$, u_{sw}, v_{iH}/v_{Ti} and v_{eH}/v_{Te}.

3.2. Finite conductivity

We are now going to determine the distribution of the potential ϕ on the dark side of the Moon for the case where the Moon has a small but finite conductivity. Since the left-hand side of (5) contains an unknown derivative $\partial\phi/\partial r$ at $r = r_m$, we first need to discuss the distribution of the potential ϕ inside the Moon. As the conductivity is assumed to be infinite at $r \leqslant r_1$, the potential ϕ at $r \leqslant r_1$ should be constant. The equation for this potential in the region $r_1 < r < r_m$ takes the form

$$\frac{1}{r}\frac{\partial}{\partial r}\left[r\sigma(r)\frac{\partial\phi}{\partial r} \right] + \frac{\sigma(r)}{r^2}\frac{\partial^2\phi}{\partial\theta^2} = 0. \tag{17}$$

Here $\sigma(r)$ is modelled by $\sigma(r) = \sigma_m \exp[(r_m - r)/\Delta r]$, where Δr is a characteristic scale of the conductivity variations inside the Moon. It is convenient to present the solution of (17) as a sum

$$\phi = \bar{\phi} + \sum_{n=1} R_n(r) \cos n\theta, \tag{18}$$

where $\bar{\phi}$ is a constant equal to the averaged potential on the surface of the Moon. It can be determined from the condition that the total flux of ions (both on the sunlit side and the dark side) penetrating into the Moon is equal to the flux of electrons.

https://doi.org/10.1017/S0022377802001654 Published online by Cambridge University Press

The solution of (17) for the radial parts R_n with the corresponding boundary condition at $r = r_1$ allows us to obtain the approximate value of the derivative $\partial\phi/\partial r$ at $r = r_m$:

$$\left.\frac{\partial\phi}{\partial r}\right|_{r_m} \approx \frac{\phi - \bar{\phi}}{\Delta r}. \tag{19}$$

As a result, we arrive at the following approximate equation for ϕ:

$$\sigma_m \frac{\phi - \bar{\phi}}{\Delta r} = e[J_{er}(\theta, \phi) - J_{ir}(\theta)]. \tag{20}$$

It is convenient to single out the undisturbed plasma concentration N_0 and the thermal velocities v_{Te} and v_{Ti} in the radial fluxes of electrons $J_e = N_0 v_{Te}\rho_e$ and protons $J_i = N_0 v_{Ti}\rho_i$, and to present (20) in the form

$$\eta^2\left(F + \frac{e\bar{\phi}}{T_e}\right) + \rho_e(F, \theta) = \frac{v_{Ti}}{v_{Te}}\rho_i(\theta), \tag{21}$$

where η^2 is a small dimensionless parameter

$$\eta^2 = \frac{\sigma_m(r_m)v_{Te}}{\epsilon_0\omega_{Pe}^2\Delta r}, \tag{22}$$

ω_{Pe} is the plasma frequency in the solar wind and ϵ_0 is the permeability of the vacuum. By substituting into (22) typical values of σ_m, v_{Te} and ω_{Pe}, we find that $\eta^2 \ll 1$ (a numerical estimate gives a value $\eta^2 \sim 10^{-5}$–10^{-6}). This allows us to use the local relation (15) for angles θ that are not too small, while

$$\eta^2\left|F + \frac{e\bar{\phi}}{T_e}\right| \ll \frac{v_{Ti}}{v_{Te}}\rho_i. \tag{23}$$

With decreasing angle θ, the flux of ions also decreases rapidly. This results in violation of the condition (23) for some angles $\theta < \theta_*$. To determine the limiting angle θ_*, we must substitute the approximate value (16) of the function F into (23). At such angles $\theta \sim \theta_*$, the function F is large enough compared with its averaged value $e\bar{\phi}/T_e$, which can be omitted from (21). Thus, the required angle θ_* is easily determined by the equation

$$\sin\theta_* \tan^5\theta_* = 4.5U_{i,2}^5\frac{\eta^2}{\mu_i}\frac{v_{Te}}{v_{iH}}\frac{v_{eH}^2}{v_{Te}^2}\left(\frac{v_{eH}}{v_{iH}}\right)^{1/4}. \tag{24}$$

To estimate the angle θ_* quantitatively, we substitute into (24) $\eta^2 = 10^{-6}$, $U_{i,2} = 3.5$, $v_{Te} = 2800\,\mathrm{km\,s^{-1}}$, $v_{Ti} = 25\,\mathrm{km\,s^{-1}}$, $v_{iH} = 100\,\mathrm{km\,s^{-1}}$ and $\mu_i \approx 10^{-1}$, and find $\theta_* \approx 65°$. The potential F for angles $\theta < \theta_*$ is determined by the relation (21) in which the flux of ions is neglected and only the main term in the electron flux is retained:

$$\eta^2 F = 0.1\mu_e \sin\theta\frac{v_{eH}^9}{v_{Te}^9}\frac{1}{F^4}. \tag{25}$$

The solution of this equation takes the form

$$F = \left(\frac{0.1\mu_e}{\eta^2}\frac{v_{eH}^9}{v_{Te}^9}\right)^{1/5}\sin^{1/5}\theta. \tag{26}$$

According to (26), the dimensionless potential F slowly decreases with θ. Its value

https://doi.org/10.1017/S0022377802001654 Published online by Cambridge University Press

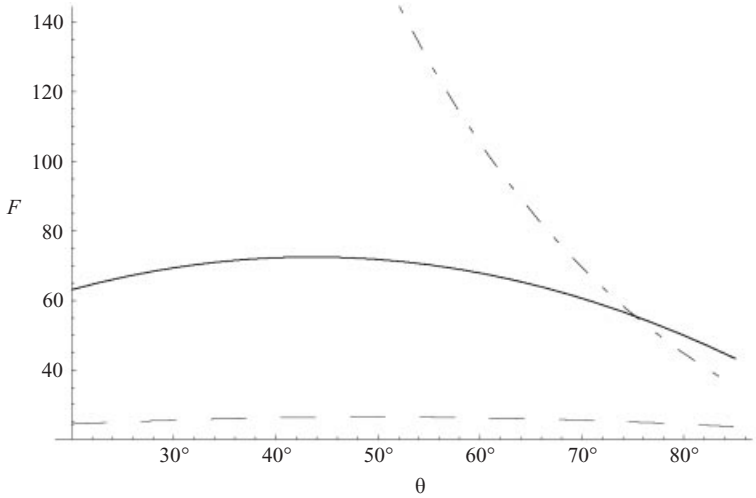


Figure 3. The dependence of the dimensionless potential $F = -e\phi/T_e$ on the conductivity at the surface of the Moon $\sigma_m(r_m)$. The solid line corresponds to $\sigma_m = 10^{-9}\,\mathrm{S\,m^{-1}}$, the dashed line to $\sigma_m = 5\times 10^{-8}\,\mathrm{S\,m^{-1}}$ and the dash-dotted line to $\sigma_m = 0$. The other parameters are as follows: $v_{Te} = 2800\,\mathrm{km\,s^{-1}}$, $v_{eH} = 4v_{Te}$, $v_{Ti} = 25\,\mathrm{km\,s^{-1}}$, $v_{iH} = 4v_{Ti}$ and $u_{sw} = 410\,\mathrm{km\,s^{-1}}$.

$F \approx 82\sin^{1/5}\theta$ is obtained after substituting in (26) the corresponding values of the main parameters ($\eta^2 \approx 10^{-6}$, $v_{eH}/v_{Te} \approx 4$ and $\mu_e \approx 0.14$). More accurately, the behavior of the potential F as a function of θ can be calculated numerically. In Fig. 3, the potential F is shown for different conductivities of the Moon: $\sigma_m = 0$ (dotted line), $\sigma_m = 5\times 10^{-8}\,\mathrm{S\,m^{-1}}$ (dot-dashed line) and $\sigma_m = 10^{-9}\,\mathrm{S\,m^{-1}}$ (solid line). It is seen clearly that even a very small conductivity of the lunar crust $\sigma_m(r_m) = 10^{-9}\,\mathrm{S\,m^{-1}}$ changes the solution very dramatically. Instead of increasing to infinity (as is the case if $\sigma_m = 0$), the potential F changes rather slowly for a wide range of θ. An increase in the conductivity by a factor of 50 causes a decrease in the potential F by a factor of two to four. According to our calculations, for conductivities $\sigma_m(r_m) \geqslant 5\times 10^{-8}\,\mathrm{S\,m^{-1}}$, the electric potential at the far side of the Moon is almost constant. This means that, even at such small conductivities, the far side of the Moon behaves like a conductor, since the fluxes of the charged particles (primarily the ions) at the far side are low enough but, at the same time, the electric potential is rather large. The potential F depends also on the characteristic velocities $v_{\alpha H}$ ($\alpha = i, e$). A decrease in v_{iH} causes a corresponding increase in the potential F at the far side of the Moon. This result is illustrated in Fig. 4 for different values of the dimensional parameter $U_{i,2}$: $U_{i,2} = 3, 5$ and $U_{i,2} = 5, 6$, and for a fixed conductivity of the Moon's crust $\sigma_m(r_m) = 10^{-9}\,\mathrm{S}$. Note that our numerical results are in agreement with those obtained above from analytical predictions of the behavior of the potential F for different conductivities $\sigma_m(r_m)$ and angles θ.

The approximate solution obtained above for F is not valid near $\theta \approx 0$, where a rapid change in the potential F is expected. For this case, our approach makes only a qualitative prediction about the magnitude of the potential F at small angles θ.

https://doi.org/10.1017/S0022377802001654 Published online by Cambridge University Press

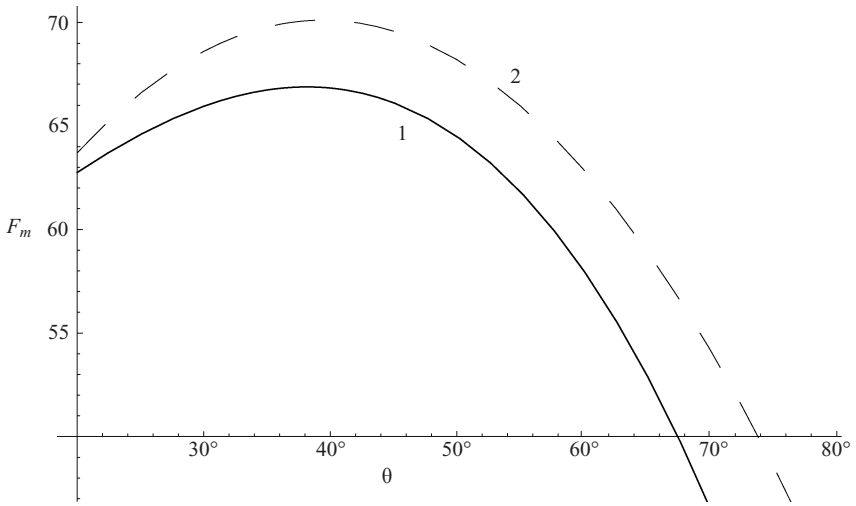


Figure 4. The influence of the ratio v_{iH}/v_{Ti} on the potential F_m at the far side of the Moon. The solid line corresponds to $v_{iH}/v_{Ti} = 4$ and the dashed line to $v_{iH}/v_{Ti} = 2.5$. The other parameters are as follows: $\sigma_m(r_m) = 10^{-9}\,\mathrm{S\,m^{-1}}$, $u_{sw} = 490\,\mathrm{km\,s^{-1}}$, $v_{Te} = 2800\,\mathrm{km\,s^{-1}}$ and $v_{Ti} = 25\,\mathrm{km\,s^{-1}}$.

4. Formation of the double layer behind the Moon

The electric potential near the far side of the Moon is determined by the Poisson equation

$$\boldsymbol{\nabla}^2\phi = -\frac{e}{\epsilon_0}[n_i(\mathbf{r}) - n_e(\mathbf{r})], \tag{27}$$

where n_i and n_e are plasma concentrations of ions and electrons, which can be calculated with the help of the corresponding distribution functions. As previously discussed, we use the guiding center approximation to calculate the trajectories of electrons. The ions are considered again as free particles. The cylindrical coordinates of a given point near the surface are $(r_m + \delta r, \theta)$, where $\delta r/r_m \ll 1$. The limiting speed of ions along the magnetic field line $v_{z,m}$ to reach the point $(r_m + \delta r, \theta)$ is

$$v_{z,m}^{(i)} = -\frac{u_{sw} + v_x}{\tan[\theta + (2\delta r/r_m)^{1/2}]}. \tag{28}$$

Since the absolute value of the speed $|v_{z,m}|$ is large for almost all $\theta \neq \pi/2$, the influence of the potential ϕ on the motion of ions is neglected. When integrating the distribution function (3) with respect to v_z, we consider the influence of the speed v_x in (28) as a small correction $|v_x/u_{sw}| \ll 1$ that can be omitted in the first approximation. As a result, the reduced concentration of ions near the far side of the Moon is presented approximately in the form

$$\frac{n_i}{N_0} = \frac{1}{2}\mathrm{Erfc}\left(\frac{U_{i,1}}{\tan\vartheta}\right) + \mu_i f_i\left(\frac{U_{i,2}}{\tan\vartheta}\right). \tag{29}$$

Here

$$\vartheta = \theta + \left(\frac{2\delta r}{r_m}\right)^{1/2}, \qquad f_i(x) = \frac{1}{\sqrt{\pi}}\int_x^\infty \frac{1}{(z^2+1)^3}\,dz,$$

https://doi.org/10.1017/S0022377802001654 Published online by Cambridge University Press

We consider the trajectories of electrons near the far side of the Moon in the guiding center approximation. The limiting speed of electrons $v_{z,m}^{(e)}$ that reach the point (x, z) near the far side of the Moon is determined by (11) with the unknown potential $\phi(x, z)$. It is convenient to introduce again the dimensionless parameters $\zeta_{e,1}^{(m)}$ and $\zeta_{e,2}^{(m)}$ associated with the speed $v_{z,m}^{(e)}$.

The reduced concentration of electrons takes the form

$$\frac{n_e}{N_0} = \frac{e^{-F}}{2}\mathrm{Erfc}(\zeta_{e,1}^{(m)}) + \mu_e f_e(\zeta_{e,2}^{(m)}), \tag{30}$$

where

$$f_e(x) = \frac{1}{\sqrt{\pi}}\int_x^\infty \frac{1}{(z^2 + 1 + Fv_{Te}^2/v_{eH}^2)^5}\,dz.$$

As the dimensionless speeds $U_{e,1}$ and $U_{e,2}$ are very small $U_{e,1} \ll 1$, $U_{e,2} \ll 1$, we can substitute approximately in (30) $\zeta_{e,1}^{(m)} = 0$ and $\zeta_{e,2}^{(m)} = 0$ for almost all angles ϑ. Using the dimensionless potential F and the coordinate $\xi = r/r_m$, the Poisson equation then reads

$$\frac{r_d^2}{r_m^2}\left(\frac{\partial^2 F}{\partial \xi^2} + \frac{1}{\xi}\frac{\partial F}{\partial \xi} + \frac{1}{\xi^2}\frac{\partial^2 F}{\partial \theta^2}\right) = \frac{1}{N_0}[n_i(\xi, \theta) - n_e(\xi, F, \theta)], \tag{31}$$

where we denote by $r_d = v_{Te}/\omega_{Pe}$ the Debye radius in the undisturbed solar wind plasma. Note that the parameter r_d^2/r_m^2 is very small: $r_d^2/r_m^2 \sim 4 \times 10^{-10}$. This means that there should be a rather wide range of coordinates (ξ, θ) where the left-hand side of (31) can be neglected, so that a simpler local relation can be used to determine the distribution of the potential F:

$$n_i(\xi, \theta) \approx n_e(\xi, F, \theta). \tag{32}$$

To determine the thickness of the double layer now, we first need to find the potential F on the side of the double layer, where quasineutrality holds. To obtain F, we simply equate the electron and proton densities.

For those angles θ that are not too close to $\pi/2$, only fast particles contribute to the reduced plasma concentrations near the far side of the Moon. This leads us to the following approximate expressions for the reduced concentrations of ions and electrons:

$$\frac{n_i}{N_0} \approx 0.1\mu_i \frac{\tan^5 \vartheta}{U_{i,2}^5}, \qquad \vartheta < \arctan U_{i,2}, \tag{33}$$

$$\frac{n_e}{N_0} \approx 0.24\mu_e \frac{1}{(1 + v_{Te}^2/v_{eH}^2 F)^{9/2}}. \tag{34}$$

The expression (34) is valid if $\vartheta \geqslant U_{e,2}$, i.e. for practically all angles θ, since $U_{e,2} \ll 1$. After substituting into (31) the reduced plasma concentrations (33) and (34), we are able to find, in explicit form, the potential F:

$$F(\xi, \theta) \approx 1.3\frac{v_{eH}^2}{v_{Te}^2}\left(\frac{U_{i,2}}{\tan \vartheta}\right)^{10/9} - \frac{v_{eH}^2}{v_{Te}^2}. \tag{35}$$

Note that for the chosen power law spectra ($n = 5$, $m = 3$), we obtain $\mu_e \approx 1.4\mu_i$. The approximate solution (35) is valid if the left-hand side of (31) is much smaller than the terms on the right-hand side. Having found F, we want to determine the

https://doi.org/10.1017/S0022377802001654 Published online by Cambridge University Press

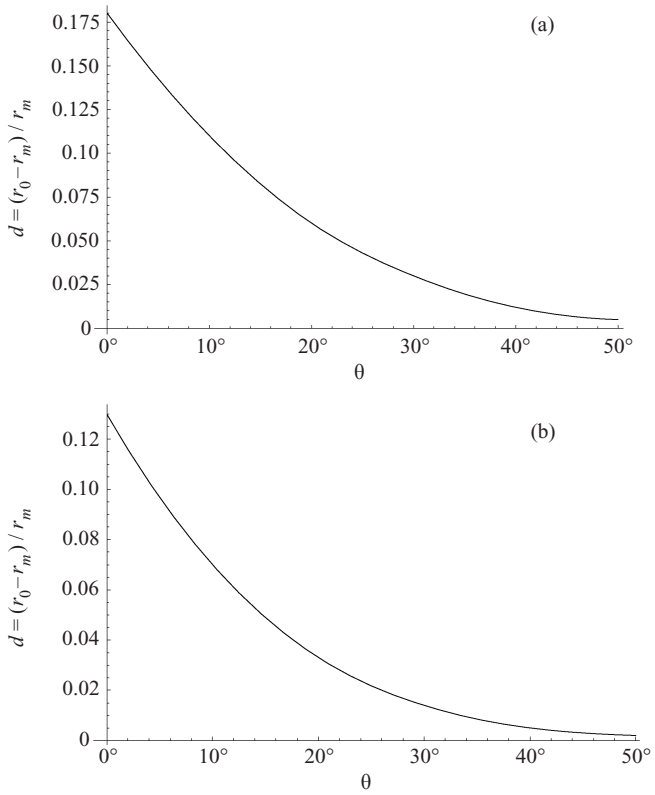


Figure 5. The thickness of the double layer as a function of the angle θ for different solar wind velocities: (a) $u_{sw} = 490\,\mathrm{km\,s^{-1}}$; (b) $u_{sw} = 350\,\mathrm{km\,s^{-1}}$. The other parameters are as follows: $v_{eH}/v_{Te} = 2.5$, $v_{iH}/v_{Ti} = 4$ and $\sigma_m(r_m) = 10^{-9}\,\mathrm{S\,m^{-1}}$.

distance ξ_0 where the quasineutrality condition breaks down. By substituting the result (35) into (31), we find the required condition:

$$\frac{1}{(\xi-1)^{3/2}} + \frac{2.8\cos\vartheta}{(\xi-1)\sin\vartheta} \ll 0.15\frac{v_{Te}^2}{v_{eH}^2}\frac{\mu_i}{U_{i,2}^6}\frac{r_m^2}{r_d^2}\sin^2\vartheta\tan^5\vartheta. \tag{36}$$

As long as this condition holds, the plasma can be considered as quasineutral. The corresponding limiting distance ξ_0 for $\mu_i = 0.1$ and $r_m/r_d = 5.8 \times 10^4$ is then determined by the equation

$$\frac{\sin\vartheta(\xi_0)}{(\xi_0-1)^{3/2}} + \frac{2.8\cos\vartheta(\xi_0)}{\xi_0-1} = 5\times10^7\frac{v_{Te}^2}{v_{eH}^2U_{i,2}^6}\sin^3\vartheta(\xi_0)\tan^5\vartheta(\xi_0). \tag{37}$$

The solution of (37), $\xi_0 = \xi_0(\theta)$, was calculated numerically. The results for different solar wind speeds ($u_{sw} = 490\,\mathrm{km\,s^{-1}}$ and $350\,\mathrm{km\,s^{-1}}$) are presented in Figs 5(a, b). It is seen that the higher the solar wind speed, the broader the double layer is at the far side of the Moon. At the same time, according to Fig. 5, the plasma can be considered as quasineutral even at rather small distances from the Moon.

The magnitude of the dimensionless potential F as a function of θ at the rear side of the double layer $\xi = \xi_0$ can be found with the help of (35) and (37). The behavior of the potential F as a function of θ for $\xi = \xi_0$, $F_0(\theta) = F(\xi_0, \theta)$ is presented in Fig. 6(a) for $u_{sw} = 490\,\mathrm{km\,s^{-1}}$ and in Fig. 6(b) for $u_{sw} = 350\,\mathrm{km\,s^{-1}}$ ($v_{iH}/v_{Ti} = 4$

https://doi.org/10.1017/S0022377802001654 Published online by Cambridge University Press

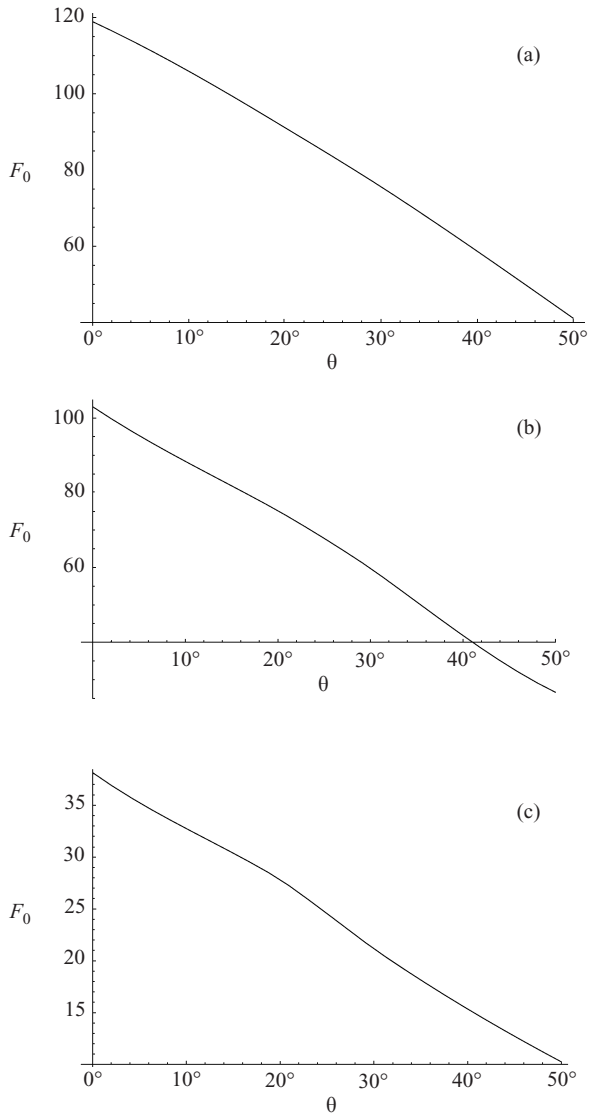


Figure 6. The dimensionless electric potential at the rear boundary of the double layer F_0 as a function of θ for different parameters: (a) $u_{sw} = 490\,\mathrm{km\,s^{-1}}$, $v_{iH}/v_{Ti} = 4$ and $v_{eH}/v_{Te} = 4$; (b) $u_{sw} = 390\,\mathrm{km\,s^{-1}}$, $v_{iH}/v_{Ti} = 4$ and $v_{eH}/v_{Te} = 4$; (c) $u_{sw} = 350\,\mathrm{km\,s^{-1}}$, $v_{iH}/v_{Ti} = 4$ and $v_{eH}/v_{Te} = 2.5$.

and $v_{eH}/v_{Te} = 4$) and in Fig. 6(c) for $u_{sw} = 350\,\mathrm{km\,s^{-1}}$ ($v_{iH}/v_{Ti} = 2.5$ and $v_{eH}/v_{Te} = 2.5$). According to Fig. 6, the potential F grows in magnitude with decreasing angle θ. The smaller the solar wind velocity u_{sw}, the smaller is the potential F. The simultaneous and equal decrease of the ratios v_{iH}/v_{Ti} and v_{eH}/v_{Te} also causes a substantial decrease in the potential F at the rear boundary of the double layer.

Closer to the Moon, where $\xi < \xi_0$, the condition (36) is violated, since only very fast ions can reach this region and hence the concentration of ions becomes too

https://doi.org/10.1017/S0022377802001654 Published online by Cambridge University Press

small. To find the potential inside the double layer, we need to use the more general equation (31) with $n_i \approx 0$. Note that the coordinates (θ, ξ) enter the right-hand side of (31) in the same combination ϑ. It is clear from the expression $\vartheta = \theta + \sqrt{2}(\xi - 1)^{1/2}$ that the solution is more sensitive to small variations of ξ than to small variations of θ. This means that we can seek a solution for the ordinary differential equation with respect to ξ while θ is considered as a parameter. Therefore, we start with the equation

$$\frac{r_d^2}{r_m^2}\left(\frac{d^2F}{d\xi^2} + \frac{1}{\xi}\frac{dF}{d\xi}\right) + \frac{n_e}{N_0}(\xi, F, \theta) = 0. \tag{38}$$

Equation (38) describes the distribution of the electric potential in the double layer behind the Moon. Two boundary conditions should be added to this equation. The first is $F(\xi_0) = F_0(\theta)$, where F_0 is the solution (35) for $\xi = \xi_0$. The second boundary condition corresponds to the potential at the far side of the Moon $F(\xi = 1) = F_m(\theta)$. After substituting the reduced electron concentration into (38), we arrive at the following ordinary nonlinear differential equation for F:

$$\frac{r_d^2}{r_m^2}\left(\frac{d^2F}{d\xi^2} + \frac{1}{\xi}\frac{dF}{d\xi}\right) + 0.24\mu_e \frac{1}{(1 + v_{Te}^2/v_{eH}^2 F)^{9/2}} = 0. \tag{39}$$

Introducing instead of F a new function

$$T = 1 + \frac{v_{Te}^2}{v_{eH}^2}F$$

and a new coordinate

$$\xi_1 = \frac{r_m}{r_d}\frac{v_{Te}}{v_{eH}}\sqrt{0.24\mu_e}\xi,$$

we arrive at the equation

$$\frac{d^2T}{d\xi_1^2} + \frac{1}{\xi_1}\frac{dT}{d\xi_1} + \frac{1}{T^{9/2}} = 0. \tag{40}$$

Assuming that in the double layer the function T changes rather quickly with ξ_1, we omit the first-order derivative in (40). After this point, it becomes easier to solve (40). First, we multiply (40) by $dT/d\xi_1$ and integrate once with respect to ξ_1. The result takes the form

$$\left(\frac{dT}{d\xi_1}\right)^2 = \frac{4}{7T^{7/2}} + T_1, \tag{41}$$

where $T_1(\theta)$ is one of the unknown functions of θ that it is necessary to add to the solution to fulfill the boundary condition. Equation (41) contains two solutions: one corresponds to the growth of the function T with the distance ξ_1, while the other describes the decreasing function.

In comparing Figs 3 and 6, we see that the ratio of the potentials F on the surface and at the rear boundary of the double layer F_m/F_0 depends on the conductivity of the Moon's crust. If the Moon's crust is treated as an insulator $\sigma_m(r_m) = 0$, then the potential F on the surface is larger than at the boundary of the quasineutral zone for all angles θ. For high enough conductivity $\sigma_m(r_m) \geqslant 5 \times 10^{-8}\,\mathrm{S\,m^{-1}}$, the opposite relation $F_m/F_0 < 1$ holds for all angles θ. For intermediate conductivities, there is a range of angles $\theta < \theta_0$ where the potential F is smaller on the surface $\xi = 1$ than at the boundary of the quasineutral zone $\xi = \xi_0$. Hence, for such angles,

https://doi.org/10.1017/S0022377802001654 Published online by Cambridge University Press

we choose the solution of (41) with the positive derivative:

$$\frac{dT}{d\xi_1} = \sqrt{\frac{4}{7T^{7/2}} + T_1(\theta)}. \tag{42}$$

The function T at a given point ξ can be found by numerical integration of (42):

$$\int_{T_m(\theta)}^{T(\xi,\theta)} \frac{U^{7/4}}{\sqrt{4 + 7T_1(\theta)U^{7/2}}}\, dU = 0.07 \frac{r_m}{r_d} \frac{v_{Te}}{v_{eH}} (\xi - 1). \tag{43}$$

Here $T_m(\theta) = 1 + (v_{Te}^2/v_{eH}^2)F_m(\theta)$ corresponds to the potential F_m on the dark side of the Moon (see Fig. 3). The coefficient on the right-hand side of (43) arises by using a value $\mu_e = 0.14$ and by returning to the coordinate ξ. A simple analytical solution follows from (43) if $T_1 > T^{-7/2}$ in the region of integration:

$$T(\xi, \theta) \approx 0.18 \frac{r_m}{r_d} \frac{v_{Te}}{v_{eH}} \sqrt{T_1(\theta)}(\xi - 1) + T_m(\theta). \tag{44}$$

This result means that the potential F in the double layer behind the Moon for the angles $\theta < \theta_0$ increases monotonically from $F_m(\theta)$ on the surface up to the value $F_0(\theta)$ at ξ_0 where the plasma becomes quasineutral. At the same time, the electric potential $\phi = -T_e F/e$ becomes smaller. The value of the function $T_1(\theta)$ is obtained with the help of (44):

$$T_1(\theta) = 31 \frac{v_{Te}^2}{v_{eH}^2} \frac{r_d^2}{r_m^2} \left(\frac{F_0 - F_m}{\xi_0 - 1} \right)^2. \tag{45}$$

After substituting in (45) the values F_m, F_0 and ξ_0 from Figs 3, 6 and 5, we find that for angles $\theta \leqslant 40^\circ$ and small enough conductivities σ_m, the function T_1 exceeds $T^{-7/2}$, and hence our analytical results (44) and (45) are approximately valid. Note that according to Figs 3 and 6, for rather large angles $\theta > \theta_0$ and conductivity $\sigma_m(r_m) = 10^{-9}\,\mathrm{S\,m^{-1}}$, the inverse relation between potentials on the surface and at the rear boundary of the double layer holds. This means that for larger angles, another solution (the one with the negative derivative) of (41) should be selected to describe the distribution of the electric potential near the Moon. It is clear from (41) that if we do not neglect the influence of the term $4/(7T^{-7/2})$ on the right-hand side, the absolute value of the derivative $dT/d\xi_1$ becomes larger and hence the thickness of the double layer decreases. Note also that the relation between the electric potentials on the surface and at the rear boundary of the double layer depends on first the conductivity of the lunar crust and second the distribution functions of charged particles. As we have mentioned above, when $\sigma_m \to 0$, the potential F_m on the surface is larger than at the rear boundary of the double layer for all angles θ (compare Figs 3 and 6).

The distribution of the potential F obtained above allows us to calculate the electron concentration in the double layer. Since the main contribution is made by fast electrons, the result is given by (34). With the help of (44) and (45), we find the distribution of electrons near the far side of the Moon:

$$\frac{n_e}{N_0} = \frac{0.24\mu_e}{\left\{ 1 + \dfrac{v_{Te}^2}{v_{eH}^2} \left[(F_0 - F_m) \dfrac{\xi - 1}{\xi_0 - 1} + F_m \right] \right\}^{9/2}}. \tag{46}$$

For angles $\theta < \theta_0$ and a conductivity $\sigma_m(r_m) = 10^{-9}\,\mathrm{S\,m^{-1}}$, according to our results, the potential F on the surface is smaller than at the rear boundary of the

https://doi.org/10.1017/S0022377802001654 Published online by Cambridge University Press

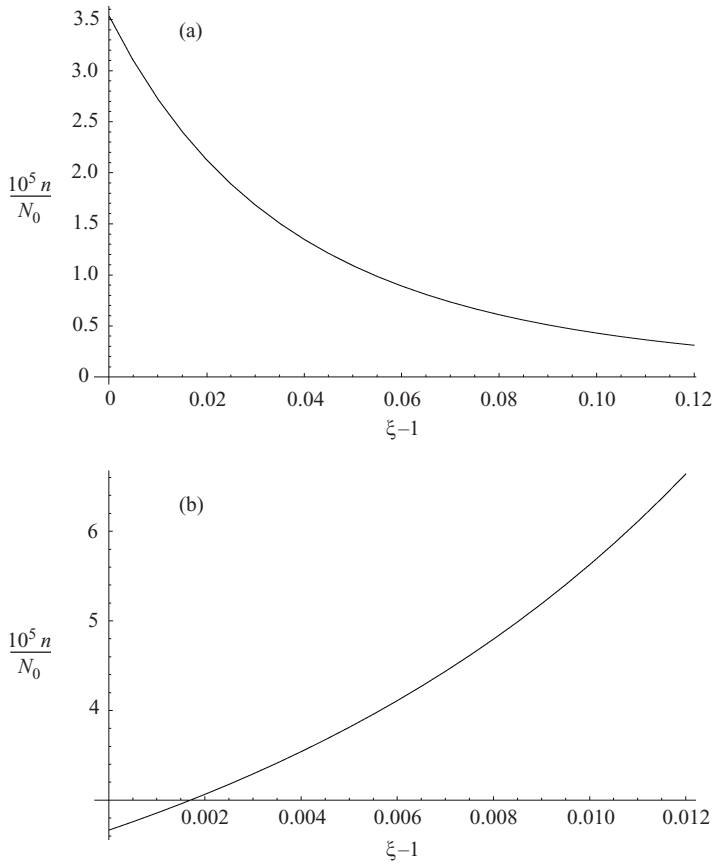


Figure 7. The variation of the reduced electron concentration in the double layer as a function of the dimensionless distance ξ for different conductivities of the lunar crust: (a) $\sigma_m = 10^{-9}\,\mathrm{S\,m^{-1}}$; (b) $\sigma_m = 5 \times 10^{-8}\,\mathrm{S\,m^{-1}}$.

double layer: $F_m < F_0$. In this case, it is clearly seen from (46) that the electron concentration decreases in the double layer with increasing distance from the Moon. For larger angles $\theta > \theta_0$, the opposite relation between potentials on the surface and at the boundary of the quasineutral zone holds: $F_m < F_0$. Because of this, the electron concentration increases in the double layer. The reduced electron concentration in the double layer as a function of a distance ξ for different angles θ is presented in Figs 7(a, b). Note that the double layer is rather thin. Its transverse scale d is much smaller than the radius of the Moon: $d \leqslant 0.2 r_m$. It decreases rapidly with increasing angle θ. The electric potential in the double layer is negative and its typical absolute values are one to two orders of magnitude larger than the electron temperature. For the chosen values of the main parameters, the expected concentration of electrons in the double layer is approximately four orders of magnitude smaller that in the solar wind. It should be mentioned that the conductivity of the lunar crust σ_m significantly influences the distribution of the electric potential in the whole double layer. As $\sigma_m \to 0$, the potential F decreases everywhere in the double layer with growing distance ξ. But, for small finite conductivity, the value of F increases with ξ within the range of angles $|\theta| \leqslant \theta_0$. Because of this,

https://doi.org/10.1017/S0022377802001654 Published online by Cambridge University Press

the electron concentration n_e, according to (34), decreases for $|\theta| \leqslant \theta_0$. For larger distances from the Moon, $\xi > \xi_0$, the concentration of charged particles begins to grow slowly. Hence, a strong depletion in the concentration of electrons appears rather close to the Moon, $\xi \sim \xi_0$, at angles $|\theta| \leqslant \theta_0$.

Our results are valid for angles ϑ that are not too small, while $U_{e,2}/\tan\vartheta \ll 1$. When ϑ goes to zero, a more general equation is required to determine the potential F:

$$\frac{r_d^2}{r_m^2}\left(\frac{\partial^2 F}{\partial \xi^2} + \frac{1}{\xi}\frac{\partial F}{\partial \xi} + \frac{1}{\xi^2}\frac{\partial^2 F}{\partial \theta^2}\right) + \frac{n_e}{N_0}(\xi, \theta, F) = 0, \tag{47}$$

where n_e contains the contribution of electron fluxes entering the wake from opposite directions along the z axis.

5. Electron fluxes near the far side of the Moon

Electron fluxes near the far side of the Moon were measured for the first time by the Apollo 15 subsatellite (Anderson et al. 1972). Recently, more detailed experimental results were obtained by Lunar Prospector (Lin et al. 1998). According to Lin et al. (1998), the flux of 40 eV electrons behind the Moon is approximately three orders of magnitude smaller than in the solar wind. For higher electron energies, the decrease is less pronounced, and for 3 keV electrons, the flux behind the Moon is slightly less than in the solar wind. Until now, no theoretical analysis of these experimental results has been given. Based on our theory, we are now able to calculate electron fluxes for different energies and compare them with the experimental data.

In connection with the experimental results (Anderson et al. 1972; Lin et al. 1998), two important points should be kept in mind. First, the distribution function of electrons definitely deviates from a Maxwellian. Otherwise, the electron fluxes that correspond to high energies would decrease behind the Moon similarly (as e^{-F}) when compared with the fluxes of the same energy ranges in the solar wind. Second, the characteristic energy of suprathermal electrons in the distribution function should not be too high compared with the dimensionless electric potential: $v_{eH}^2/v_{Te}^2 < F$. If the energy of the suprathermal electrons is sufficiently high, i.e. $v_{eH}^2/v_{Te}^2 \gg F$, the ratio of fluxes along the magnetic field line at the far side and in the solar wind depend only slightly on the energy (see (48) below).

We now apply our model to calculate electron fluxes behind the Moon. The magnetic field of the solar wind is assumed, at the moment, to be orthogonal to the solar wind flow velocity. Such a case was indeed observed by the Apollo 15 subsatellite and presented by Anderson et al. (1972). For simplicity, we restrict ourselves to the high-energy part of the spectra and assume that the energy range ΔW that contributes to the flux at a given energy W is considerably smaller than the energy W (more correctly, $\Delta W < 2/nW$). In this case, the ratio of the electron fluxes behind the Moon to the electron flux in the solar wind can be written approximately as

$$R = \frac{J_e^{(0)}(W)}{J_e^{(1)}(W)} = \frac{(1 + \zeta_e^2 + F v_{Te}^2/v_{eH}^2)^n}{(1+\zeta_e^2)^n}. \tag{48}$$

Here $J_e^{(0)}(W)$ is the flux of suprathermal electrons in the solar wind with energy W, $J_e^{(1)}(W)$ is the electron flux with the same energy behind the Moon and $\zeta_e = \sqrt{W}/\sqrt{m}v_{eH}$. According to (48), the ratio of the electron fluxes depends on three

https://doi.org/10.1017/S0022377802001654 Published online by Cambridge University Press

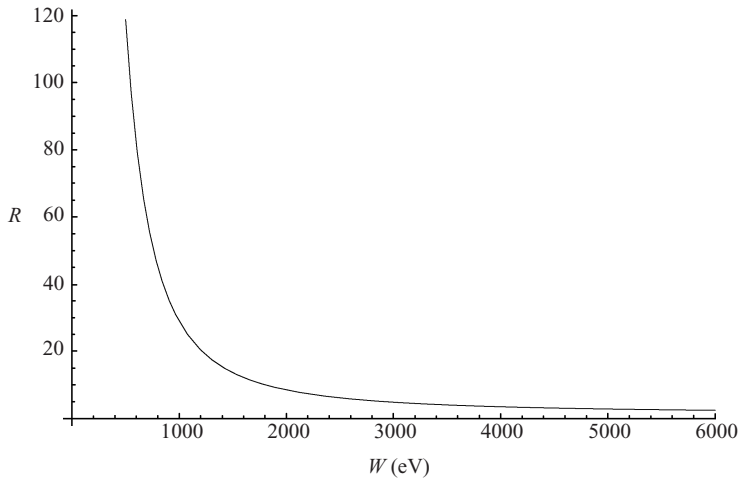


Figure 8. The ratio of electron fluxes in the undisturbed solar wind and behind the Moon as a function of energy for $u_{sw} = 350\,\mathrm{km\,s^{-1}}$ and $v_{eH}/v_{Te} = 2.5$.

main parameters: the electric potential along the trajectory of the satellite F and the parameters n and v_{eH}/v_{Te} of the electron distribution function. The electric potential, in turn, depends on the solar wind velocity, the distribution functions of ions and electrons, and the conductivity of the Moon's crust. It follows from (48) that for high enough energies $W > 2nFW_{Te}$, the ratio $R(W, F)$ tends towards unity as

$$R \approx 1 + 2nF\frac{W_{Te}}{W}, \tag{49}$$

where $W_{Te} = mv_{Te}^2/2$. To estimate the effect numerically, we need to substitute into (48) the values of the three parameters F, n and v_{eH}/v_{Te}. Their exact values are unknown for the cases analyzed by Anderson et al. (1972) and Lin et al. (1998). To match the experimental results, we assume that the ratio of the characteristic suprathermal velocity v_{eH} and the electron thermal velocity v_{Te} is $v_{eH}/v_{Te} = 2.5$. The solar wind speed is taken to be $u_{sw} = 350\,\mathrm{km\,s^{-1}}$. The parameter n that determines the spectrum of suprathermal electrons is chosen, as previously discussed, to be $n = 5$. The thickness of the double layer for $u_{sw} = 350\,\mathrm{km\,s^{-1}}$ is shown in Fig. 5(b), while the electric potential F at the boundary of the quasineutral zone is given in Fig. 6(c).

According to Fig. 5(b), the thickness of the double layer behind the Moon at small angles θ is about $d \approx 200\,\mathrm{km}$ and its magnitude, according to Fig. 6(c), is $F \approx 40$. Closer to the Moon, at a distance of order 100 km and for angles $\theta \approx 0$, the potential F should be smaller. For our calculations, we choose a value of $F = 30$. We present the flux ratios R calculated with the help of (48) in Fig. 8, which shows that this ratio is large for small energies and decreases rapidly with energy W. For example, the calculated ratio of electron fluxes for an energy $W = 40\,\mathrm{eV}$ is $R \approx 3.5 \times 10^3$, while for an energy $W = 3\,\mathrm{keV}$, this ratio is only $R \approx 4.8$. Measurements made by Lunar Prospector show that the flux ratio at an energy $W = 40\,\mathrm{eV}$ was of order 10^3, while at an energy $W = 2.95\,\mathrm{keV}$, it was only of order 10. We conclude that our results presented in Fig. 8 are in rather good qualitative agreement with the available experimental data obtained by the Apollo 15 subsatellite and Lunar

https://doi.org/10.1017/S0022377802001654 Published online by Cambridge University Press

Prospector, taking into account that we do not know the exact values for the main parameters.

The important point of our analysis is that our theory links the different parameters describing the Moon–solar wind interaction on the far side of the Moon. Knowing some of these parameters, we are able to estimate within our model the parameters that are not directly measured by experiment, such as the conductivity of the Moon's crust. If flux ratios are measured at different distances from the Moon, the distribution of the electric potential ϕ near the far side of the Moon can be found from the data. This is seen by reversing (48):

$$F(\mathbf{r}) = [R^{1/n}(W, \mathbf{r}) - 1] \left(\frac{v_{eH}^2}{v_{Te}^2} + \frac{W}{m v_{Te}^2} \right), \tag{50}$$

where $F(\mathbf{r})$ is the dimensionless electric potential at point $\mathbf{r}$.

6. Influence of the direction of the solar magnetic field on the electric potential

We have so far discussed the special case where the solar magnetic field is orthogonal to the flow velocity $\mathbf{u}_{sw}$. Now we suppose that there is an arbitrary angle in the ecliptic plane between the directions of the solar wind velocity and the magnetic field. It is convenient to introduce two systems of coordinates: the first, (x, z), is associated with the solar wind flow velocity (the x axis is parallel to the vector $\mathbf{u}_{sw}$), while the second, (x_1, z_1), is connected with the direction of the magnetic field (the z_1 axis coincides with the direction of the magnetic field). Let α be the angle between the x and x_1 axes. The limiting speed of ions considered as free particles along the magnetic field line to reach a certain point on the far side of the Moon is given by

$$v_{z_1,m}^{(i)} = -\left[u_{sw} \frac{\cos\theta}{\sin(\theta + \alpha)} + \frac{v_{x_1}}{\tan(\theta + \alpha)} \right]. \tag{51}$$

Here the angle θ is calculated, as previously discussed, from the x axis. Equation (51) means that the domain of integration with respect to the velocities v_{z_1} and x_{x_1} to obtain the radial flux of ions that reach the far side of the Moon is determined by

$$v_{z_1} \sin(\alpha + \theta) + v_{x,1} \cos(\alpha + \theta) \leqslant -u_{sw} \cos\theta. \tag{52}$$

With the help of (52), we can find the radial flux of ions in the form

$$\begin{aligned} J_{ir}(\theta) = &-\frac{N_0}{\sqrt{2}\pi} v_{Ti} \cos(\theta + \alpha) \int_0^\infty e^{-\tilde{\zeta}_{i,1}^2} [e^{-\tilde{\chi}_{i,1}^2} - \sqrt{\pi}\tilde{\chi}_{i,1} \operatorname{Erfc}(\tilde{\chi}_{i,1})]\, d\tilde{\zeta}_{i,1} \\ &-\mu_i \frac{N_0}{\sqrt{2}\pi} v_{iH} \cos(\theta + \alpha) \int_0^\infty \frac{1}{(\tilde{\zeta}_{i,2}^2 + 1)^3} [e^{-\tilde{\chi}_{i,2}^2} - \sqrt{\pi}\tilde{\chi}_{i,2} \operatorname{Erfc}(\tilde{\chi}_{i,2})]\, d\tilde{\zeta}_{i,2}. \end{aligned} \tag{53}$$

Here

$$\tilde{\zeta}_{i,1} = -\frac{v_{z_1}}{\sqrt{2} v_{Ti}}, \qquad \tilde{\zeta}_{i,2} = -\frac{v_{z_1}}{\sqrt{2} v_{iH}},$$

$$\tilde{\chi}_{i,1} = U_{i,1} \frac{\cos\theta}{\cos(\theta + \alpha)} - \tilde{\zeta}_{i,1} \tan(\theta + \alpha), \qquad \tilde{\chi}_{i,2} = U_{i,2} \frac{\cos\theta}{\cos(\theta + \alpha)} - \tilde{\zeta}_{i,2} \tan(\theta + \alpha).$$

If $\alpha = 0$, the result (53) coincides with (8). Now we briefly discuss the expression for the normal component of the electron flux. Once again, we use the guiding center

https://doi.org/10.1017/S0022377802001654 Published online by Cambridge University Press

approximation. As a result, we arrive at the following expression for the radial electron flux:

$$J_{er} = -\frac{N_0 v_{Te}}{\sqrt{2}\pi} e^{e\phi/T_e} \cos(\theta+\alpha) \int_{\tilde{\zeta}_{e,1}^{(m)}}^{\infty} e^{-\tilde{\zeta}_{e,1}^2} [e^{-\tilde{\chi}_{e,1}^2} - \sqrt{\pi}\tilde{\chi}_{e,1} \operatorname{Erfc}(\tilde{\chi}_{e,1})]\, d\tilde{\zeta}_{e,1}$$
$$-\mu_e \frac{N_0}{\sqrt{2}\pi} v_{eH} \cos(\theta+\alpha) \int_{\tilde{\zeta}_{e,2}^{(m)}}^{\infty} \frac{[e^{-\tilde{\chi}_{e,2}^2} - \sqrt{\pi}\tilde{\chi}_{e,2} \operatorname{Erfc}(\tilde{\chi}_{e,2})]^{-1}}{(\tilde{\zeta}_{e,2}^2 - e\phi/T_{eH} + 1)^5}\, d\tilde{\zeta}_{e,2}. \quad (54)$$

Here

$$\tilde{\zeta}_{e,1}^{(m)} = -\frac{v_{z1,m}^{(e)}}{\sqrt{2}v_{Te}}, \qquad \tilde{\zeta}_{e,2}^{(m)} = -\frac{v_{z1,m}^{(e)}}{\sqrt{2}v_{eH}},$$
$$\tilde{\zeta}_{e,1} = -\frac{v_{z_1}}{\sqrt{2}v_{Te}}, \qquad \tilde{\zeta}_{e,2} = -\frac{v_{z_1}}{\sqrt{2}v_{eH}},$$
$$\tilde{\chi}_{e,1} = U_{e,1}\frac{\cos\theta}{\cos(\theta+\alpha)} - \tilde{\zeta}_{e,1}\tan(\theta+\alpha), \qquad \tilde{\chi}_{e,2} = U_{e,2}\frac{\cos\theta}{\cos(\theta+\alpha)} - \tilde{\zeta}_{e,2}\tan(\theta+\alpha).$$

The exact values of the limiting velocities $\tilde{\zeta}_{e,1}^{(m)}$ and $\tilde{\zeta}_{e,2}^{(m)}$ are difficult to present in explicit form due to the unknown distribution of the electric potential ϕ. Nevertheless, we can expect that these velocities are of the order of

$$\tilde{\zeta}_{e,1}^{(m)} \sim U_{e,1}\frac{\cos\theta}{\sin(\theta+\alpha)}, \qquad \tilde{\zeta}_{e,2}^{(m)} \sim U_{e,2}\frac{\cos\theta}{\sin(\theta+\alpha)}. \quad (55)$$

As previously discussed, it is possible to find approximate analytical expressions for the fluxes of ions and electrons. The main term describing the radial flux of ions takes the form

$$J_{ir} \approx -\frac{\mu_i N_0}{2\sqrt{2\pi}} v_{iH} \frac{\sin^5(\theta+\alpha)}{[U_{i,2}^2\cos^2\theta + \sin^2(\theta+\alpha)]^2}. \quad (56)$$

For $\alpha = 0$, the expression (56) coincides with one of the terms in (9) that represents the flux of suprathermal protons. Similarly, the main contribution from the flux of suprathermal electrons is given by

$$J_{er} \approx -\frac{\mu_e N_0}{4\sqrt{2\pi}} v_{eH} \frac{\sin(\theta+\alpha)}{(1 + F v_{Te}^2/v_{eH}^2)^4}. \quad (57)$$

By equating the fluxes of ions (56) and electrons (57), we obtain the distribution of the electric potential on the far side of the Moon:

$$F \approx \frac{v_{eH}^2}{v_{Te}^2}\left[\left(\frac{\mu_e v_{eH}}{2\mu_i v_{iH}}\right)^{1/4} \frac{[U_{i,2}^2\cos^2\theta + \sin^2(\theta+\alpha)]^{1/2}}{\sin(\theta+\alpha)} - 1\right]. \quad (58)$$

If the angle θ is not very close to $\pi/2$, and hence $U_{i,2}|\cos\theta| \gg |\sin(\theta+\alpha)|$, the result (58) reduces to

$$F \approx \frac{v_{eH}^2}{v_{Te}^2}\left(\frac{\mu_e v_{eH}}{2\mu_i v_{iH}}\right)^{1/4} U_{i,2}\frac{\cos\theta}{\sin(\theta+\alpha)}. \quad (59)$$

The main distinction between the results (59) and (16) is the lack of symmetry for the angles $\theta = \pi/2$ and $\theta = -\pi/2$. For a fixed θ, the potential (59) can be larger or smaller (depending on the sign of α) than in the case previously discussed. The approximate result (59) is not valid if the angle $\theta + \alpha$ is too small. In this case,

https://doi.org/10.1017/S0022377802001654 Published online by Cambridge University Press

the finite conductivity of the lunar crust must be taken into account. The limiting angle θ_* is determined by the following equation (compare with (24)):

$$\frac{\sin^6(\theta_* + \alpha)}{\cos^5 \theta_*} = 4.5 U_{i,2}^5 \frac{\eta^2}{\mu_i} \frac{v_{Te}}{v_{iH}} \frac{v_{eH}^2}{v_{Te}^2} \left(\frac{v_{eH}}{v_{iH}} \right)^{1/4}. \tag{60}$$

7. Summary and discussion

In this paper, the distribution of plasma and electric fields near the far side of the Moon is investigated. We have discussed the formation of a double layer behind the Moon and have estimated its parameters. It has been shown that due to the suprathermal tails in the distribution of electrons and protons in the solar wind, the double layer should be thin. The electric potential in the layer is rather high (much higher than the temperature of electrons) – but not as large as was predicted previously for large cosmic bodies (Gurevich and Pitaevskii 1965). The existence of a small but finite conductivity of the lunar crust contributes significantly to the distribution of the electric potential at the far side of the Moon and determines the electric currents flowing along the magnetic field lines and close to the Moon's interior. We have estimated, theoretically, electron fluxes behind the Moon for different frequency ranges and compared them with the experimental data obtained recently by Lunar Prospector and previously by the Apollo 15 subsatellite. In our analysis, it was assumed that all charged particles that reach the surface of the Moon are absorbed. It is possible to consider a more general case when the reflection coefficient from the surface is not equal to zero. Note that the local increase in the electron reflection coefficient was measured by Lunar Prospector and was explained by the action of surface crustal magnetic fields (Lin et al. 1998). In addition, in our approach, we are able to include electric currents connected with the creation of charged particles due to the bombardment of the surface by micrometeorits and the electric charging of dust.

According to our theory, the distribution of plasma and electric fields near the far side of the Moon depends on several main parameters: the characteristic thermal (v_{Te} and v_{Ti}) and suprathermal (v_{eH} and v_{iH}) speeds of electrons and protons, the speed of the solar wind u_{sw} and its direction with respect to the magnetic field (angle α), the parameters n and m that describe suprathermal tails in the distributions of electrons and ions, and, last of all, the distribution of conductivity $\sigma_m(r)$ inside the Moon. Most of these parameters change over time. Our numerical calculations show that the results are rather sensitive to the variations of the main parameters (e.g. the ratios v_{Ti}/v_{iH} and v_{Te}/v_{eH}, the solar wind velocity u_{sw}, and the conductivity of the Moon's crust). To make accurate theoretical predictions, one should know the values of the above-mentioned parameters. For this reason, the forthcoming missions SMART 1 and SELENE will provide valuable information for theoretical analysis of the physical processes near the far side of the Moon.

References

Al'pert, Ya. L., Gurevich, A. V. and Pitaevskii, L. P. 1965 *Space Physics with Artificial Satellites*. New York: Consultants Bureau.

Anderson, K. A., Chase, L. M., Lin, R. P., McCoy, J. E. and McGuire, R. F. 1972 *J. Geophys. Res.* **77**, 4611.

https://doi.org/10.1017/S0022377802001654 Published online by Cambridge University Press

Astudillo, H. F., Livi, S., Marsch, E. and Rosenbauer, H. 1996 *J. Geophys. Res.* **101**, 24 423.
Dyal, P., Parkin, C. W. and Daily, W. D. 1974 *Rev. Geophys. Space Phys.* **12**, 568.
Freeman, J. W., Fenner, M. Jr. and Hills, H. K. 1973 *J. Geophys. Res.* **78**, 4560.
Gloecker, G., Geiss, J., Balsiger, H., Bedini, P., Cain, J. C., Fisher, J. et al. 1992 *Astron. Astrophys. Suppl. Ser.* **92**, 267.
Goldstein, B. E. 1974 *J. Geophys. Res.* **79**, 23.
Grobman, W. D. and Blank, J. L. 1969 *J. Geophys. Res.* **74**, 3943.
Gurevich, A. V. and Pitaevskii, L. P. 1965 In: *Reviews of Plasma Physics*, Vol. 1 (ed. M. A. Leontovich). New York: Consultants Bureau, p. 1.
Kuckes, A. F. 1971 *Nature* **232**, 249.
Lin, R. P., Mitchell, D. L., Curtis, D. W., Anderson, K. A., Carlson, C. W., McFadden, J. et al. 1998 *Science* **281**, 1480.
Ogilvie, K. W., Steinberg, J. T., Fitzenreiter, R. J., Owen, C. J., Lazarus, A. J., Farrell, W. M. and Torbert, R. B. 1996 *Geophys. Res. Lett.* **23**, 1255.
Pilipp, W. G., Miggenrieder, H., Montgomery, M. D., Mülhäuser, K.-H., Rosenbauer, H. and Schwenn, R. 1987 *J. Geophys. Res.* **92**, 1075.
Sonett, C. P. and Mihalov, J. D. 1972 *J. Geophys. Res.* **77**, 588.

https://doi.org/10.1017/S0022377802001654 Published online by Cambridge University Press